

Glass formation in binary alloys with different atomic symmetries

Yuan-Chao Hu,¹ Kai Zhang,² Sebastian A. Kube,¹ Jan Schroers,¹ Mark D. Shattuck,³ and Corey S. O'Hern^{1,4,5,*}

¹*Department of Mechanical Engineering & Materials Science,
Yale University, New Haven, Connecticut 06520, USA*

²*Division of Natural and Applied Sciences, Duke Kunshan University, Kunshan, Jiangsu, 215300, China*

³*Benjamin Levich Institute and Physics Department,
The City College of New York, New York, New York 10031, USA.*

⁴*Department of Physics, Yale University, New Haven, Connecticut 06520, USA.*

⁵*Department of Applied Physics, Yale University, New Haven, Connecticut 06520, USA.*

(Dated: January 17, 2022)

Prediction of the glass forming ability (GFA) of alloys remains a major challenge. We are not able to predict the composition dependence of the GFA of even binary alloys. To investigate the effect of each element's propensity to form particular crystal structures on glass formation, we focus on binary alloys composed of elements with the same size, but different atomic symmetries using the patchy-particle model. For mixtures with atomic symmetries that promote different crystal structures, the minimum critical cooling rate R_c is only a factor of 5 lower than that for the pure substances. For mixtures with different atomic symmetries that promote local crystalline and icosahedral order, the minimum R_c is more than 3 orders of magnitude lower than that for pure substances. Results for R_c for the patchy-particle model are in agreement with those from embedded atom method simulations and sputtering experiments of NiCu, TiAl, and high entropy alloys.

Bulk metallic glasses (BMGs), which are multi-component alloys with disordered atomic-scale structure, are a promising materials class because they combine metal-like strength with plastic-like processability [1, 2]. Despite their potential, they have not been widely used, likely because current BMGs do not combine multiple advantageous properties, such as high strength, high fracture toughness, and low material cost [3–6].

A first step in the BMG design process is the ability to predict the glass-forming ability (GFA), or critical cooling rate R_c below which crystallization occurs. BMGs with good GFA, e.g. $\text{Pd}_{42.5}\text{Cu}_{30}\text{Ni}_{7.5}\text{P}_{20}$ with $R_c \sim 10^{-2}$ K/s, have been identified mainly through time-consuming experiments that are guided by empirical rules [7, 8]. The number of alloys that can potentially form metallic glasses is enormous, *i.e.* more than 10^6 for four-component alloys with 32 possible elements and 1% increments in composition of the four elements [6]. However, even using the latest high-throughput sputtering techniques, researchers can only characterize a minute fraction of these [9–12].

We seek to develop a computational platform to predict the GFA of alloys. We focus on binary systems (with elements A and B) and determine whether the best GFA occurs for equal proportions of A and B, or for the A- or B-rich systems. The answer to even this simple question is unknown for most binary alloys. Prior studies have focused on the role of atomic size and cohesive energy in determining the GFA of alloys [14, 15, 18]. Other studies suggest that the composition with the best GFA can be predicted from the equilibrium liquidus curve [17, 19]. However, many alloys do not possess eutectic points, and there are numerous examples where the composition with the best GFA deviates from the deepest eutectic [4, 20, 21]. Few studies have considered the effect

of each element's propensity to form particular crystal structures on the GFA of alloys.

To simplify the problem, we consider binary alloys for which the atomic radii are the same, and investigate how the GFA depends on the competing crystalline phases of the pure substances. We first investigated the GFA of two specific binary alloys, NiCu and TiAl, using MD simulations of embedded atom method (EAM) potentials to determine R_c versus alloy composition [22, 23]. When the pure substances crystallize, Ni and Cu form face-centered cubic (FCC) crystals; Ti forms hexagonal close packed (HCP) and Al forms FCC crystals in equilibrium. (Details of the EAM simulations are provided in the Supplemental Materials (SM) [24].) We show in Fig. 1 (a) that R_c for NiCu varies by less than a factor of 5 over the full range of composition. In contrast, R_c for TiAl decreases by more than three orders of magnitude as the fraction of Al is increased. We find similar results for the GFA of NiCu and TiAl alloys in co-sputtering experiments, which correspond to $R \sim 10^9$ K/s (Fig. 1 (b)). (See SM for experimental details.) We observe only crystallized samples for NiCu over the full range of compositions, whereas there is a wide range of compositions where amorphous samples occur for TiAl. Although we have not determined the compositions with the best GFA in these two alloys, Fig. 1 (b) demonstrates the large difference in their GFA.

Although Al crystallizes into FCC structures in equilibrium, experimental studies have shown that Al-based BMGs possess local icosahedral order centered on the Al atoms and form metastable quasicrystals [25–27]. In addition, EAM simulations have shown that pure Al forms quasicrystals by rapid quenching [28]. The above results for TiAl alloys suggest that mixtures of elements with crystalline and icosahedral (ICO) atomic symme-

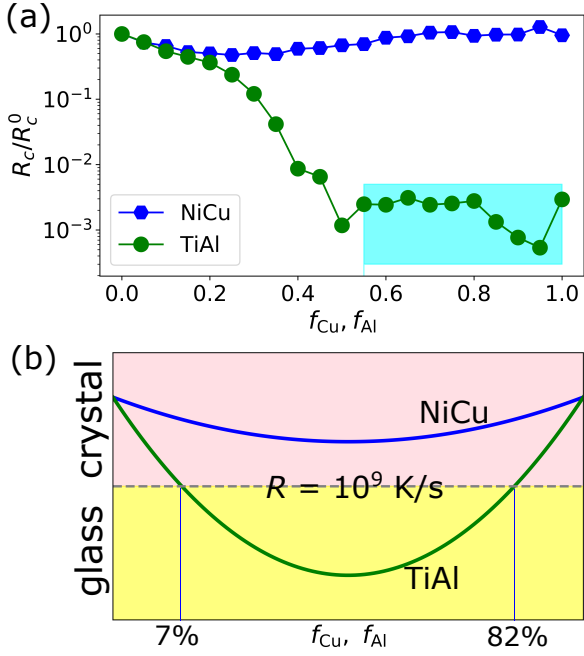


FIG. 1. (a) The critical cooling rate R_c/R_c^0 for NiCu (normalized by R_c^0 for pure Ni) versus the fraction f_{Cu} of Cu atoms, and TiAl (normalized by R_c^0 for pure Ti) versus the fraction f_{Al} of Al atoms, obtained using EAM simulations. The binary alloys with $f_{Al} \gtrsim 0.5$ (cyan region) form quasicrystals for $R < R_c$. (b) Schematic diagram of solidification for NiCu and TiAl based on co-sputtering experiments, which correspond to $R \sim 10^9$ K/s. NiCu alloys crystallize over the full range of f_{Cu} , while TiAl alloys form glasses for $0.07 < f_{Al} < 0.82$.

tries, and similar atomic sizes, can yield alloys with R_c that are several orders of magnitude lower than that for pure systems.

A limitation of EAM potentials [13] is that the atomic symmetry of the elements cannot be tuned independently, while keeping other important features, such as atomic size and cohesive energy, fixed. To overcome this limitation, we perform MD simulations of the patchy-particle model [29] for binary alloys, where small patches on the surfaces of the same types of atoms attract each other when they are aligned (and atoms of different types interact via the Lennard-Jones potential). (See SM.) Using this model, we study the GFA of binary mixtures of the same-sized atoms with different atomic symmetries (*e.g.* BCC, FCC, and HCP). Systems that contain atoms with a given symmetry crystallize with that particular symmetry at low cooling rates. In addition, we study mixtures of atoms with crystalline and ICO symmetries by controlling the number and placement of patches on the atom surfaces.

We find that the GFA of binary alloys modeled using the patchy-particle interaction possesses a minimum within $0 < f_B < 1$, whose location depends on the atomic symmetry and cohesive energies of the elements. In con-

trast, the melting temperature T_m of the crystalline solids varies approximately linearly with composition. We find that the composition with the best GFA corresponds to that for which the local icosohedral order in the liquid state is maximized. However, if the icosohedral ordering is too strong, metastable quasicrystals form, which decreases the GFA. Moreover, R_c for mixtures of atoms with different atomic symmetries and cohesive energies can be collapsed by the amount of local icosohedral order in the system.

In Fig. 2, we show R_c for binary alloys using the patchy particle model. To measure R_c , we cool the alloys linearly from the liquid state to zero temperature at rate R and define R_c as the rate below which the zero-temperature system develops strong bond orientational order. (See SM.) In (a), we consider three binary alloys with FCC-BCC, FCC-HCP, and HCP-BCC symmetries for elements A - B and the same cohesive energies $\epsilon_{AA} = \epsilon_{BB}$. Pure substances with HCP symmetry have the lowest R_c , while R_c is similar for pure substances with FCC and BCC symmetries. In general, we find that R_c is minimal for non-pure substances. For FCC-BCC binary alloys, the composition with the best GFA has $f_B \approx 0.5$. In contrast, for binary alloys containing atoms with HCP symmetry, the system with minimum R_c has

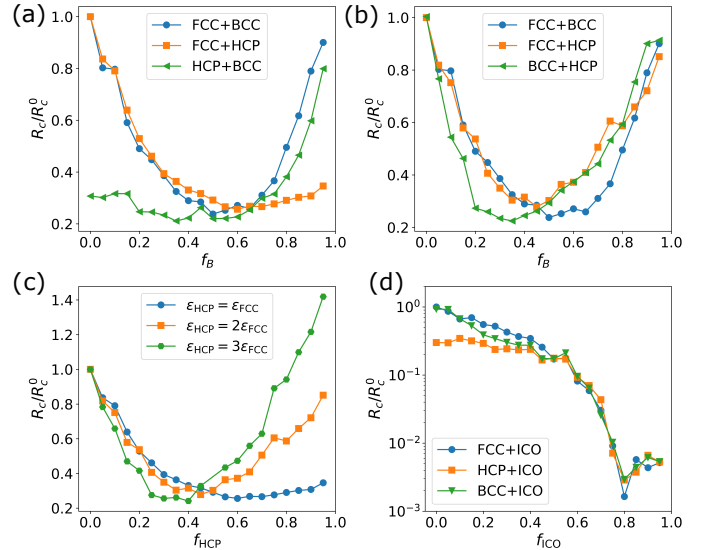


FIG. 2. R_c for binary alloys (normalized by R_c^0 for the pure system with FCC symmetry) using the patchy-particle model. (a) R_c/R_c^0 for binary mixtures with A- and B-atoms [(A: FCC, B: BCC; circles), (A: FCC, B: HCP; squares), and (A: HCP, B: BCC; triangles)] versus the fraction of B atoms f_B with $\epsilon_{BCC}/\epsilon_{FCC} = \epsilon_{HCP}/\epsilon_{FCC} = 1.0$. (b) R_c/R_c^0 for binary mixtures, where the pure substances (with FCC, BCC, or HCP symmetries) have similar R_c . We set $\epsilon_{BCC}/\epsilon_{FCC} = 1.0$ and $\epsilon_{HCP}/\epsilon_{FCC} = 2.0$. (c) R_c/R_c^0 for binary mixtures with FCC and HCP symmetries, and $\epsilon_{HCP}/\epsilon_{FCC} = 1.0, 2.0$, and 3.0. (d) R_c/R_c^0 for binary mixtures of atoms with crystalline and icosahedral symmetries and the same cohesive energies.

a majority of HCP atoms.

In Fig. 2 (b), we plot R_c for binary alloys containing atoms that have FCC, BCC, and HCP symmetries, but the pure substances have similar GFA (by varying the cohesive energies). As in Fig. 2 (a), R_c possesses a minimum in the range $0 < f_B < 1$. For binary alloys containing atoms with BCC symmetry, the system with the lowest R_c has a majority of BCC atoms. For binary alloys with atoms with FCC and HCP symmetries, $f_B \approx 0.5$ has the best GFA since FCC and HCP crystal structures are similar.

In Fig. 2 (c), we show R_c for binary alloys containing atoms with FCC and HCP symmetries versus the HCP-fraction f_{HCP} , for three cases where HCP crystals have different GFAs (by adjusting $\epsilon_{\text{HCP}}/\epsilon_{\text{FCC}}$). We find that as R_c at $f_{\text{HCP}} = 1$ decreases, f_{HCP} with the best GFA increases. These results emphasize that the location of the minimum in R_c is influenced by the GFA of the pure substances, which depends on their atomic symmetry and cohesive energy.

As shown in Fig. 2, for binary alloys containing same-sized atoms, but different crystalline symmetries, the minimum R_c changes by only a factor of 5 relative to that for the pure substances. For binary alloys with elements of the same atomic sizes *and* symmetries, we showed previously that R_c scales with the ratio of the cohesive energies of the pure substances [15, 29]. Thus, results for R_c for the patchy-particle model are in general agreement with those for EAM simulations of NiCu (with $\epsilon_{\text{Ni}}/\epsilon_{\text{Cu}} \approx 1.3$) in Fig. 1 (a), as well as experimental studies of mixtures of Ar and Kr (with $\epsilon_{\text{Kr}}/\epsilon_{\text{Ar}} \approx 1.45$) [30].

Motivated by the results for EAM simulations of TiAl in Fig. 1 (a), we show R_c for binary alloys containing atoms with ICO and different crystalline symmetries in Fig. 2 (d). R_c decreases modestly (by less than an order of magnitude) for $f_{\text{ICO}} \lesssim 0.5$, and decreases dramatically (by more than two orders of magnitude) for $0.5 \lesssim f_{\text{ICO}} \lesssim 0.8$. When $f_{\text{ICO}} \gtrsim 0.8$, the system can form quasicrystals [31], which causes R_c to increase as $f_{\text{ICO}} \rightarrow 1$. (See SM for methods to detect quasicrystals.) Note that R_c for elements with ICO symmetry is much lower than that for elements with crystalline symmetry. We find that $R_c(f_{\text{ICO}})$ possesses a minimum near $f_{\text{ICO}} \sim 0.8$. The non-monotonic behavior of $R_c(f_{\text{ICO}})$ can be rationalized by considering the interfacial free energy barrier for crystal nucleation [31–34]. In the crystal-forming regime with $f_{\text{ICO}} \lesssim 0.8$, local icosahedral order is incompatible with crystalline symmetry, and thus increasing f_{ICO} enhances the free energy barrier for crystal nucleation, leading to decreases in R_c . However, for $f_{\text{ICO}} \gtrsim 0.8$, ICO symmetry becomes compatible with quasicrystalline order, reducing the interfacial free energy barrier and increasing R_c .

Prior studies suggest that the melting temperature T_m of alloys can be used to predict R_c [19]. To test this hypothesis, we measured T_m for all binary mixtures in

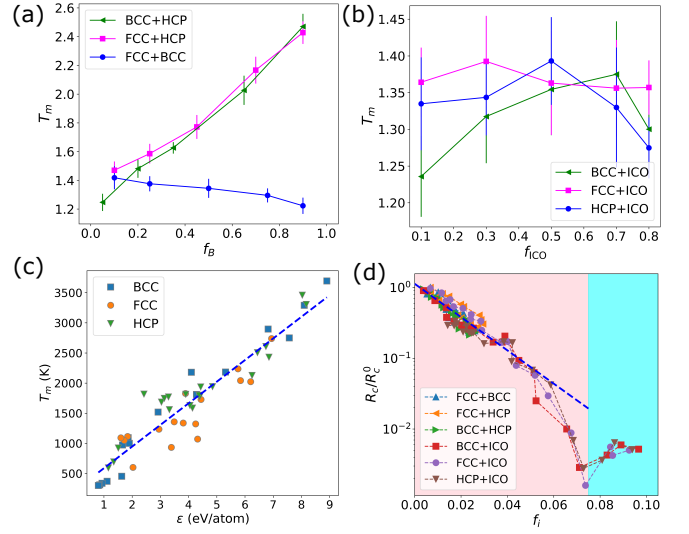


FIG. 3. (a) Melting temperature T_m for binary alloys (in units of ϵ_{AA}/k_B) using the patchy-particle model for mixtures of A- and B- atoms. The pure substances have similar R_c ; see Fig. 2 (b). (b) T_m for binary mixtures of atoms with crystalline and ICO symmetries. T_m in (a) and (b) are obtained by heating the quenched crystalline solids to high temperature at rates $R_h \sim R_c^0$. (c) T_m versus the cohesive energy per particle ϵ for 53 pure metals with BCC, FCC, and HCP symmetries in their equilibrium solid forms. The blue dashed line gives $T_m = 0.03\epsilon/k_B$, where k_B is the Boltzmann constant. (d) R_c normalized by R_c^0 for pure substances with FCC symmetry versus the fraction of atoms f_i with local icosahedral order in binary alloys using the patchy-particle model. f_i is measured at zero temperature using the lowest R at which all systems remain disordered. For $f_i \lesssim 0.075$, FCC, BCC, and HCP structures form for $R < R_c$. In the cyan region, systems form quasicrystals for $R < R_c$. The blue dashed line indicates exponential decay, $R_c/R_c^0 \sim \exp(-23.5f_i)$.

Fig. 2 [35]. In Fig. 3 (a), we show T_m for binary alloys containing atoms with different crystalline symmetries, where the pure substances have the same GFA. From experimental data in Fig. 3 (c), T_m for pure substances scales roughly linearly with the cohesive energy, although the atomic symmetry gives rise to deviations [36, 37]. Thus, T_m for binary alloys containing atoms with different crystalline symmetries is roughly linear in f_B , and the sign of the slope is determined by the sign of $\epsilon_{BB} - \epsilon_{AA}$. We contrast this behavior for $T_m(f_B)$ with that for $R_c(f_B)$, which possesses a minimum in the range $0 < f_B < 1$. In Fig. 3 (b), we show T_m for binary alloys containing atoms with ICO and crystalline symmetries. In this case, T_m is nearly constant for $f_{\text{ICO}} \gtrsim 0.5$, whereas R_c decreases by more than 2 orders of magnitude. Thus, we do not find a strong correlation between T_m and GFA in our model binary alloys.

Several studies have characterized the local structural order, such as the size and shape of Voronoi polyhedra, local bond orientational order, and changes of nearest

neighbor atoms, in glass-forming materials as they are cooled [13]. In particular, researchers have found that the number of atoms with local icosahedral order increases when good glass-formers are cooled toward the glass transition [38]. Thus, one suggestion for improving the GFA is to maximize local icosahedral order. In Fig. 3(d), we show that R_c for all of the patchy-particle systems studied collapses when plotted against the fraction f_i of atoms in the system that have local icosahedral order, where the icosahedral order is characterized using rapid quenches for which all of the systems remain disordered. (See SM for the definition of local icosahedral order.) $R_c(f_i)$ has several key features. First, for $f_i \lesssim 0.06$, where most of the data for the binary mixtures containing atoms with crystalline symmetries exists, R_c decays exponentially with increasing f_i . In the regime $0.06 \lesssim f_i \lesssim 0.075$, R_c decreases more rapidly. For $f_i \gtrsim 0.075$, since the system can form quasicrystals, R_c begins to increase. Thus, we predict non-monotonic behavior in $R_c(f_i)$.

To what extent are the results for the patchy-particle model consistent with those for the EAM simulations of NiCu and TiAl? First, in Fig. 4 (a) and (c), we show T_m versus f_{Cu} for NiCu and versus f_{Al} for TiAl alloys, which are consistent with the experimental melting curves [39]. For NiCu, T_m decreases roughly linearly from ~ 1700 K to ~ 1400 K over the range $0 < f_{Cu} < 1$. In contrast, $R_c(f_{Cu})$ for NiCu possesses a shallow minimum near $f_{Cu} \sim 0.25$. For TiAl, T_m has a small maximum at ~ 1800 K for $f_{Al} \sim 0.3$, and then T_m decreases monotonically for $f_{Al} \gtrsim 0.3$. In contrast, $R_c(f_{Al})$ decreases over the range $0 < f_{Al} < 0.5$ and has a minimum for

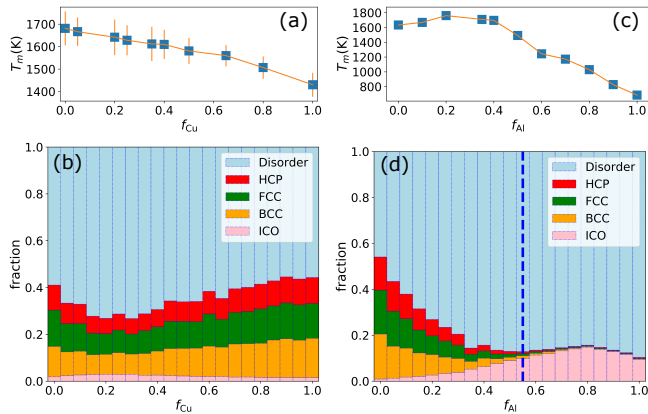


FIG. 4. (a) T_m versus f_{Cu} for EAM simulations of NiCu using $R_h = 10^{11}$ K/s. (b) Fraction of atoms with a given local order: HCP, FCC, BCC, ICO, or other disordered motifs versus f_{Cu} for zero-temperature systems at $R > R_c$. (c) T_m versus f_{Al} for EAM simulations of TiAl using $R_h = 10^{10}$ K/s. (d) Fraction of atoms with a given local order: HCP, FCC, BCC, ICO, and other disordered motifs versus f_{Al} at $R > R_c$. For $f_{Al} > 0.5$ (vertical dashed line), quasicrystals form for $R < R_c$. The local order in (b) and (d) is measured at $R \sim 10^{13}$ K/s.

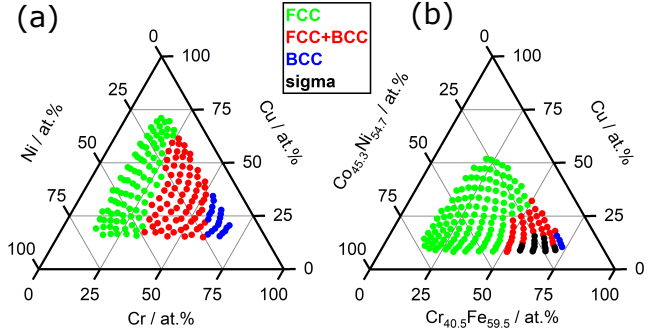


FIG. 5. Crystallization of sputtered (a) CrNiCu and (b) CrFe-CoNi-Cu alloys. In (a), systems along the binary NiCu axis form FCC crystals, in agreement with the pure substances. With increasing fraction of Cr (with BCC symmetry), the structure transitions to BCC. Crystal formation over the full composition range indicates that $R_c > 10^9$ K/s for all Cr-NiCu (and NiCu) alloys in experiments. Similarly, in (b), we find crystal formation over the full range of compositions in CrFe-CoNi-Cu alloys [40], despite several competing crystalline phases.

$f_{Al} \sim 0.9-0.95$ (although the precise location of the minimum is affected by the degree of quasicrystalline order). These results further emphasize the decoupling of T_m and R_c . Importantly, as shown in Fig. 4 (b) for NiCu and (d) for TiAl, the composition region with the best GFA is the same as that with the largest fraction of atoms with icosahedral order, and a minimal amount of (FCC, HCP, and BCC) crystalline order.

Additional results from co-sputtering experiments [40] on multi-component alloys with same-sized atoms provide further support for our findings. (See SM.) As shown in Fig. 5 (a), all compositions for NiCuCr (and NiCu) alloys crystallize for $R \sim 10^9$ K/s. We also show results in Fig. 5 (b) for the quinary alloy CrFe-CoNi-Cu. All compositions crystallize, despite the fact that the individual elements form different crystalline phases, confirming our results for the patchy-particle model for binary alloys without ICO symmetry.

In summary, we employed MD simulations of EAM potentials and the patchy-particle model to investigate the influence of atomic symmetry on the GFA of binary alloys with no atomic size differences. In general, we find that the minimum R_c does not occur for pure substances. For binary alloys containing atoms with different crystalline symmetries, the minimum R_c is only a factor of 5 lower than that for pure substances, which is consistent with recent experimental studies of binary systems, such as NiCu and ArKr, whose elements readily form FCC structures, as well as high-entropy alloys. In contrast, R_c for binary alloys containing atoms with ICO and crystalline symmetries can be reduced by three orders of magnitude relative to that for pure substances by increasing f_{ICO} . These results emphasize that GFA of binary alloys can be greatly increased by mixing elements that enhance local

icosahedral order f_i . However, $R_c(f_i)$ is not monotonic; we show that R_c possesses a minimum at a characteristic $f_i \gtrsim 0.075$, where quasicrystals form. This result may explain why it is difficult to obtain binary BMGs with large amounts of Al (since it can lead to the formation of quasicrystals), whereas minor alloying with Al can dramatically increase the GFA.

Although our results were obtained by studying binary alloys with elements of the same size, they provide insights into the GFA of alloys with elements of different sizes. For example, for CuZr, the cohesive energies satisfy $\epsilon_{\text{Zr}} > \epsilon_{\text{Cu}}$, and thus pure Cu (with FCC symmetry) is expected to have better GFA than pure Zr (with HCP symmetry). (This result is confirmed by EAM simulations in SM.) Further, Zr is larger than Cu with diameter ratio, $\sigma_{\text{Cu}}/\sigma_{\text{Zr}} = 0.8$, and based on our prior studies of binary Lennard-Jones systems [41], Cu-rich alloys (with a majority of smaller atoms) have better GFA. Thus, based on the cohesive energies and atomic sizes of Cu and Zr, the composition with the best GFA should be Cu-rich. EAM simulations for CuZr have shown that $\text{Cu}_{64}\text{Zr}_{36}$ is the composition with the best GFA, and at this composition the local icosahedral order is maximized [24, 42]. In future studies, we will perform MD simulations of models of CuZr (and other binary alloys) with effective pairwise interactions that include cohesive energy and atomic size differences to identify the most promising BMG-forming binary alloys.

ACKNOWLEDGEMENTS

The authors acknowledge support from NSF Grant Nos. DMR-1119826 (Y.-C.H.), CMMI-1901959 (C.O.), and CMMI-1463455 (M.S.). This work was supported by the High Performance Computing facilities operated by, and the staff of, the Yale Center for Research Computing. The authors thank P. Banner (Yale University), as well as S. Sarker and A. Mehta (SLAC National Accelerator Laboratory) for their contribution to the experimental studies.

* corey.ohern@yale.edu

- [1] G. Kumar, H. X. Tang, and J. Schroers, *Nature* **457**, 868 (2009).
- [2] M. Chen, *Annu. Rev. Mater. Res.* **38**, 445 (2008).
- [3] W. Johnson, *Nat. Mater.* **14**, 553 (2015).
- [4] W. H. Wang, C. Dong, and C. H. Shek, *Mater. Sci. Eng.: R: Reports* **44**, 45 (2004).
- [5] Y. Sun, A. Concustell, and A. L. Greer, *Nat. Rev. Mater.* **1**, 16039 (2016).
- [6] Y. Li, S. Zhao, Y. Liu, P. Gong, and J. Schroers, *ACS Comb. Sci.* **19**, 687 (2017).
- [7] N. Nishiyama and A. Inoue, *Appl. Phys. Lett.* **80**, 568 (2002).
- [8] A. Inoue, *Acta Mater.* **48**, 279 (2000).
- [9] S. Ding, Y. Liu, Y. Li, Z. Liu, S. Sohn, F. J. Walker, and J. Schroers, *Nat. Mater.* **13**, 494 (2014).
- [10] P. Bordeenithikasem, J. Liu, S. A. Kube, Y. Li, T. Ma, B. E. Scanley, C. C. Broadbridge, J. J. Vlassak, J. P. Singer, and J. Schroers, *Sci. Rep.* **7**, 7155 (2017).
- [11] F. Ren, L. Ward, T. Williams, K. J. Laws, C. Wolverton, J. Hattrick-Simpers, and A. Mehta, *Sci. Adv.* **4**, eaq1566 (2018).
- [12] M.-X. Li, S.-F. Zhao, Z. Lu, A. Hirata, P. Wen, H.-Y. Bai, M. Chen, J. Schroers, Y. Liu, and W.-H. Wang, *Nature* **569**, 99 (2019).
- [13] Y. Q. Cheng and E. Ma, *Prog. Mater. Sci.* **56**, 379 (2011).
- [14] K. J. Laws, D. B. Miracle, and M. Ferry, *Nat. Commun.* **6**, 8123 (2015).
- [15] Y.-C. Hu, J. Schroers, M. D. Shattuck, and C. S. O'Hern, *Phys. Rev. Mater.* **3**, 085602 (2019).
- [16] E. Perim, D. Lee, Y. Liu, C. Toher, P. Gong, Y. Li, W. N. Simmons, O. Levy, J. J. Vlassak, J. Schroers, and S. Curtarolo, *Nat. Commun.* **7** (2016).
- [17] D. Turnbull, *Contemp. Phys.* **10**, 473 (1969).
- [18] K. Zhang, M. Wang, S. Papanikolaou, Y. Liu, J. Schroers, M. D. Shattuck, and C. S. O'Hern, *J. Chem. Phys.* **139**, 124503 (2013).
- [19] W. L. Johnson, J. H. Na, and M. D. Demetriou, *Nat. Commun.* **7** (2016).
- [20] L. Xia, W. H. Li, S. S. Fang, B. C. Wei, and Y. D. Dong, *J. Appl. Phys.* **99**, 026103 (2006).
- [21] H. Tan, Y. Zhang, D. Ma, Y. P. Feng, and Y. Li, *Acta Mater.* **51**, 4551 (2003).
- [22] B. Onat and S. Durukanolu, *J. Phys. Condens. Matter* **26**, 035404 (2013).
- [23] R. R. Zope and Y. Mishin, *Phys. Rev. B* **68**, 024102 (2003).
- [24] See Supplemental Material at [URL] for MD simulation details, structural characterization methods and sputtering experimental details.
- [25] A. Inoue, *Prog. Mater. Sci.* **43**, 365 (1998).
- [26] D. Shechtman, I. Blech, D. Gratias, and J. Cahn, *Phys. Rev. Lett.* **53**, 1951 (1984).
- [27] L. C. Chen and F. Spaepen, *Nature* **336**, 366 (1988).
- [28] A. Prokhoda and A. Ovrutsky, *arXiv preprint arXiv:1403.6668* (2014).
- [29] K. Zhang, Y. Liu, J. Schroers, M. D. Shattuck, and C. S. O'Hern, *J. Chem. Phys.* **142**, 104504 (2015).
- [30] A. Schottelius, F. Mambretti, A. Kalinin, B. Beyersdorff, A. Rothkirch, C. Goy, J. Mller, N. Petridis, M. Ritzer, F. Trinter, J. M. Fernandez, T. A. Ezquerro, D. E. Galli, and R. E. Grisenti, *Nat. Mater.* **19**, 512 (2020).
- [31] A. S. Keys and S. C. Glotzer, *Phys. Rev. Lett.* **99**, 235503 (2007).
- [32] H. Tanaka, *J. Phys. Condens. Matter* **15**, L491 (2003).
- [33] H. Tanaka, *J. Non-Cryst. Solids* **351**, 678 (2005).
- [34] Y. T. Shen, T. H. Kim, A. K. Gangopadhyay, and K. F. Kelton, *Phys. Rev. Lett.* **102**, 057801 (2009).
- [35] H.-J. Lee, T. Cagin, W. L. Johnson, and W. A. Goddard, *J. Chem. Phys.* **119**, 9858 (2003).
- [36] A. M. Halpern, *J. Chem. Edu.* **89**, 592 (2012).
- [37] F. Guinea, J. H. Rose, J. R. Smith, and J. Ferrante, *Appl. Phys. Lett.* **44**, 53 (1984).
- [38] Y. Cheng, E. Ma, and H. W. Sheng, *Phys. Rev. Lett.* **102**, 245501 (2009).
- [39] J. Murray and T. Massalski, *American Society for Metals* **1**, 142 (1986).

- [40] S. A. Kube, S. Sohn, D. Uhl, A. Datye, A. Mehta, and J. Schroers, *Acta Mater.* **166**, 677 (2019).
- [41] K. Zhang, W. W. Smith, M. Wang, Y. Liu, J. Schroers, M. D. Shattuck, and C. S. O'Hern, *Phys. Rev. E* **90**, 032311 (2014).
- [42] J. Ding, Y.-Q. Cheng, and E. Ma, *Acta Mater.* **69**, 343 (2014).